Available online at www.sciencedirect.com
ScienceDirect
Journal of the European Ceramic Society 27 (2007) 207–213
www.elsevier.com/locate/jeurceramsoc

Preparation and characterization of SnO_2 and Cu-doped SnO_2 thin films using electrostatic spray deposition (ESD)

C. Matei Ghimbeu [a,b,*], R.C. van Landschoot [b], J. Schoonman [b], M. Lumbreras [a]

[a] *L.I.C.M. Groupe Capteurs, University of Metz, 1 Bd. Arago, 57078 Metz Cedex 3, France*
[b] *Delft Institute for Sustainable Energy, Delft University of Technology, Julianalaan 136, 2628 BL Delft, The Netherlands*

Received 10 February 2006; received in revised form 26 April 2006; accepted 6 May 2006
Available online 16 June 2006

Abstract

Tin (IV) oxide thin films were deposited on platinum-coated alumina substrates by means of electrostatic spray deposition (ESD) technique using as precursor solution tin chloride pentahydrate ($SnCl_4 \cdot 5H_2O$) in ethanol. The influence of the deposition parameters (temperature, time and flow rate) and copper addition on the morphology and microstructure of the films was studied using scanning electron microscopy (SEM), transmission electron microscopy (TEM), X-ray diffraction (XRD) and Raman spectroscopy, respectively. The tetragonal rutile phase is evidenced by X-ray diffraction (XRD) with no other phases observed. The size of the particles calculated from the XRD peaks are in the nanometer range (7–10 nm) which is in good agreement with the transmission electron microscopy (TEM) results. The Raman spectra indeed revealed that the SnO_2 films are crystallized in the rutile tetragonal phase and furthermore a peak shift and a decrease of the peaks intensity can be remarked for the films doped with CuO.

Keywords: Films; Electron microscopy; SnO_2; Sensors; Spray deposition

1. Introduction

SnO_2 is an interesting material due to its potential application in solar cells,[1] as conductive transparent electrode,[2] in transistors,[3] in varistors,[4] and in sensors.[5] Over the time, tin (IV) oxide (SnO_2) proved to be the most widely used semiconductor oxide gas sensor which can detect a wide range of pollutant gases.[6–10] The sensing mechanism of tin (IV) oxide, being an n-type semiconductor, is based on resistance changes if it is exposed to oxidizing or reducing gases. A major drawback of SnO_2 and metal oxide-based gas sensors is the lack of selectivity, which limits its further applications when each gas must be detected in a mixture of gases. To overcome this drawback different strategies have been employed. It is well known that the sensitivity and selectivity of SnO_2 can be improved by adding small amounts of dopants. For example, the sensitivity of SnO_2 to H_2 is improved by doping with In_2O_3,[11] to O_2 by doping with Ga_2O_3,[12] and in particular the sensitivity of SnO_2 to H_2S is improved four orders of magnitude by doping with small amount of CuO.[13]

The sensors selectivity can be improved also by using an array of sensors and evaluating the sensor response data with pattern recognition methods like principal component analysis (PCA),[14,15] discriminant factor analysis (DFA),[16,17] and artificial neural network method (ANN).[18,19] This combination between an array of sensors and a pattern recognition method led to the system known as "electronic nose". SnO_2 or doped SnO_2 as active gas sensor material is used as powder, ceramic compacts, and thick or thin films. It has been proved that the use of films presents advantages such as high mechanical resistance, easier application of the electrodes, and the possibility of miniaturization.[20] Different techniques were used to prepare SnO_2 or doped SnO_2 thin films, i.e., spray pyrolysis,[21,22] sol–gel process,[23–25] chemical vapor deposition,[26,27] sputtering,[8,28] pulsed-laser deposition.[29] In this work SnO_2 and CuO-doped SnO_2 thin films are deposited using the electrostatic spray deposition (ESD) technique which offers many advantages like simple set-up, ambient pressure operation, high deposition efficiency, and good control of the surface morphology. Tuning the ESD-deposition parameters different morphologies ranging

* Corresponding author. Tel.: +33 3 87 54 70 76; fax: +33 3 87 31 52 32.
E-mail address: camelia.matei@umail.univ-metz.fr (C.M. Ghimbeu).

0955-2219/$ – see front matter © 2006 Elsevier Ltd. All rights reserved.
doi:10.1016/j.jeurceramsoc.2006.05.092

from dense to fractal-like porous and even reticular with interconnected pores were obtained.[30,31] The aim of this work is to prepare thin films of SnO_2 and CuO-doped SnO_2 using ESD technique in order to find the best process conditions to obtain especially porous thin films suitable for gas sensor application.

2. Experimental aspects

2.1. ESD set-up

For the deposition of the films a vertical ESD set-up was used.[31] The liquid precursor is pumped by a syringe pump (Kd Scientific, model 100, USA) through a flexible tube of plastic material (Watson Marlow Marprene®, inner diameter 1.3 mm) to the tip of a stainless steel nozzle (outside diameter, 0.9 mm). When a high voltage is applied by a dc voltage power supply (FUG HCN 14-12500, Rosenheim, Germany) between the nozzle and the substrate the precursor solution is atomised into an aerosol. This aerosol consists of highly charged droplets that are attracted by the grounded and heated substrate where they impinge, loose their charge and after complete solvent evaporation the thin layer is formed on the substrate surface. The temperature of the substrate is maintained at a constant value using a temperature control unit (Eurotherm Controls, model 2216e), which includes a heating element and a temperature controller.

2.2. Films deposition

Tin chloride pentahydrate ($SnCl_4{\cdot}5H_2O$, Aldrich, 98% purity) was dissolved in absolute ethanol (C_2H_5OH, J.T. Baker, 99.9% purity) to obtain a 0.05 M precursor solution for depositing SnO_2 films. For the doping procedure a 0.05 M precursor solution of copper (II) nitrate hemipentahydrate ($Cu(NO_3)_2{\cdot}2.5H_2O$, 98% purity, Aldrich) in ethanol was used. The doping of the films was varied from 1 to 4 at.%. The precursor solutions were pumped through the metal nozzle using a flow rate of 1–4 ml h^{-1}. The substrate comprised alumina pellets (99.7%, Gimex Technische Keramiek B.V., The Netherlands), with dimension of 10 mm × 20 mm and thickness 1 mm. The substrate was then coated partially with a layer (1–5 μm) of platinum paste (Engelhard Clal, model 6082A) and fired at 800 °C for 2 h in air. This substrate was fixed in a stainless steel substrate holder, in order to allow a circular deposition surface of 10 mm in diameter (see Fig. 1).

The temperature of the substrate was varied in the range 150–400 °C and the deposition time between 1 and 3 h. A distance of 20 mm was kept between the nozzle and the substrate. A positive voltage between 6.0 and 8.5 kV was applied to the nozzle in order to generate the aerosol of the precursor solution. The film deposition took place under ambient atmosphere. The as-deposited films were annealed at 550 °C in air for 2 h to remove any possible organic rests remained from the precursor solution and also to improve the crystallinity and to sinter the layer.

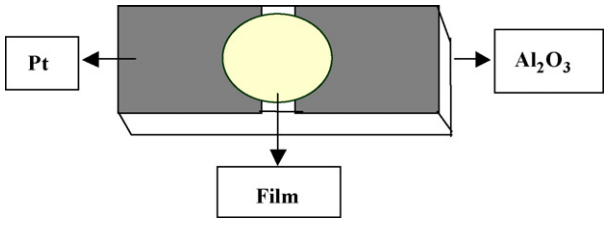

Fig. 1. Schematic representation of the films deposited on Pt-coated alumina.

2.3. Structure characterization techniques

The surface morphology and the thickness of the coatings were investigated using a JOEL JSM 580 LV scanning electron microscope (SEM). To determine the films thicknesses and to avoid charging of the samples a thin film of gold was sputtered on the surface using an Edwards Sputter Coater S150 B.

The transmission electron microscopy (TEM) measurements were performed using a PHILIPS CM30T electron microscope with a filament of LaB_6. The system is operating at 300 kV. The samples are placed on Quantifoil carbon polymer supported on a gold grid by applying a few droplets of ground sample with ethanol, followed by drying in air. The chemical analysis of the thin films was investigated using an energy dispersive X-ray (EDX) analyzer (Oxford Instruments).

The crystal structure of the films was determined with a Bruker D8 Advance X-ray diffractometer (XRD) using monochromatic Cu Kα radiation (λ = 1.5406 Å, 40 kV and 40 mA).

Raman measurements were performed at room temperature using a home-built set-up. The excitation source used is an Nd:YVO_4 laser system (Spectra Physics Millennia), which is working at a wavelength of 532 nm. The spectra were recorded in the back-scatter mode using a liquid-nitrogen cooled CCD camera (Princeton Instruments LN/CCD-1100PB) connected with a Spex 340E monochromator. The monochromator is equipped with an 1800 grooves/mm grating. The CCD chip is controlled by a Princeton Instruments ST-138 controller, which is connected to a personal computer running with WinSpec software. The laser beam power on the sample was limitated to ∼2 mW to prevent heating of the samples. The scattering is removed effectively with two notch filters (Kaiser Optical Systems).

3. Results and discussion

The SnO_2 morphology changes as a function of the substrate temperature (Fig. 2) was first studied. If the film is deposited at 150 °C (Fig. 2a) the droplets arriving at the substrate do not evaporate on the surface and a dense smooth film is formed. Nevertheless, the film presents cracks, probably caused by thermal stress built-up during the drying process of the film. In the same experiment repeated at 250 °C (Fig. 2b) the film becomes denser. This film comprised of large particles of about 1 μm, which are agglomerates of small particles. No cracks are observed in this case. If the deposition temperature is further increased up to 350 and 400 °C (Fig. 2c and d) a porous layer is formed due to the faster growth rate. As can be seen (Fig. 2) the particle sizes decrease with the increase of the deposition temperature. Also

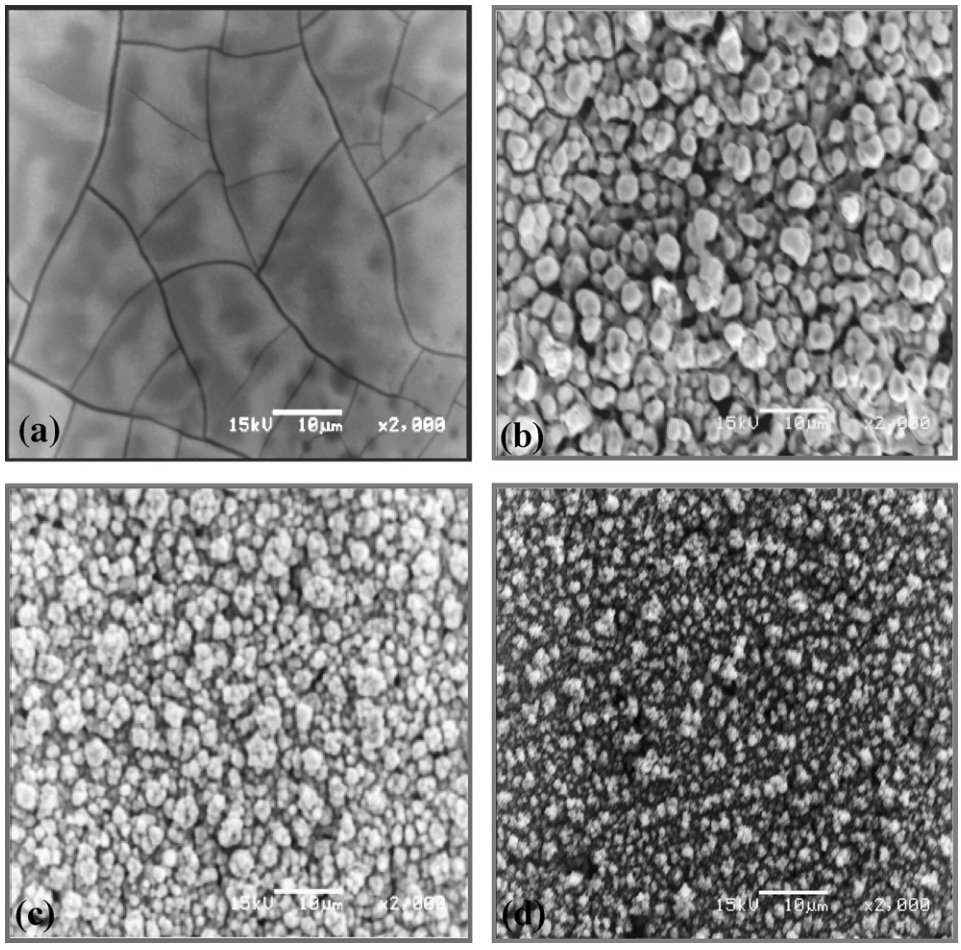

Fig. 2. SEM pictures of SnO_2 films deposited with 1 ml/h for 1 h using different deposition temperatures: (a) 150 °C; (b) 250 °C; (c) 350 °C; (d) 400 °C.

the porosity and roughness increase with increasing temperature.

The effect of the deposition time on the morphology of the SnO_2 films has also been studied. Fig. 3a shows that the films deposited in 1 h have a thickness of 5–6 μm. This was determined from the film cross-section (Fig. 3a′). With increase of the deposition time up to 3 h (Fig. 3b) the layer thickness increases to 20–25 μm (see Fig. 3b′). The porosity of these films also increases. The change in the porosity can be explained by the fact that in the first case the particles arriving at the substrate are spreading easily on the alumina substrate, therefore, a denser layer is formed. When the deposition time is increased, the arriving droplets have to spread on the surface of the already deposited layer and discrete particles are formed which increase the roughness and lead to a more porous morphology.

Fig. 4 presents the SEM pictures of the SnO_2 layers deposited at 400 °C, using a range of flow rates from 1 to 4 ml/h. For a low flow rate (Fig. 4a and b) a porous film is formed due to the fact that the particles arriving at the substrate are dry or semi-dry and slightly spread over the substrate.

As can be observed, the size of the particles is increasing with the increase of the flow rate of the precursor solution. When the droplets are landing on the substrate, they are still wet, spread over it and a denser film is formed (Fig. 4c). Nevertheless, the films that show a high porosity have a low adhesion to the substrate, a fact observed also by Chen et al.[30] In this way a compromise between porosity and adhesion can be obtained in order to have good quality SnO_2 thin films.

For the deposition of the SnO_2 films doped with CuO the parameters, which lead to a porous morphology as well as a good adherence to the substrate are used (Fig. 4b).

Furthermore, the influence of the Cu dopant on the morphology of the films is studied. The process of doping does not have a significant influence on the morphology. The morphology studies of the layer show a porous structure in which the primary particles are present in aggregates, which have sizes in the range 1–5 μm in diameter. This porous morphology is preferred for gas sensor applications, because of large adsorption areas for the gas molecules. As can be seen, the aggregates are uniformly distributed. The thickness of the film determined by the SEM cross-section (Fig. 4d) is about 7–8 μm.

TEM pictures of SnO_2 (Fig. 5a) revealed that the particle dimensions are ranging between 10 and 15 nm. The grain size of un doped SnO_2 was found to be similar to that of Cu-doped SnO_2 (Fig. 5b) and small amounts of Cu have little influence on film morphology and particle size. This fact is also found in the present SEM and XRD studies.

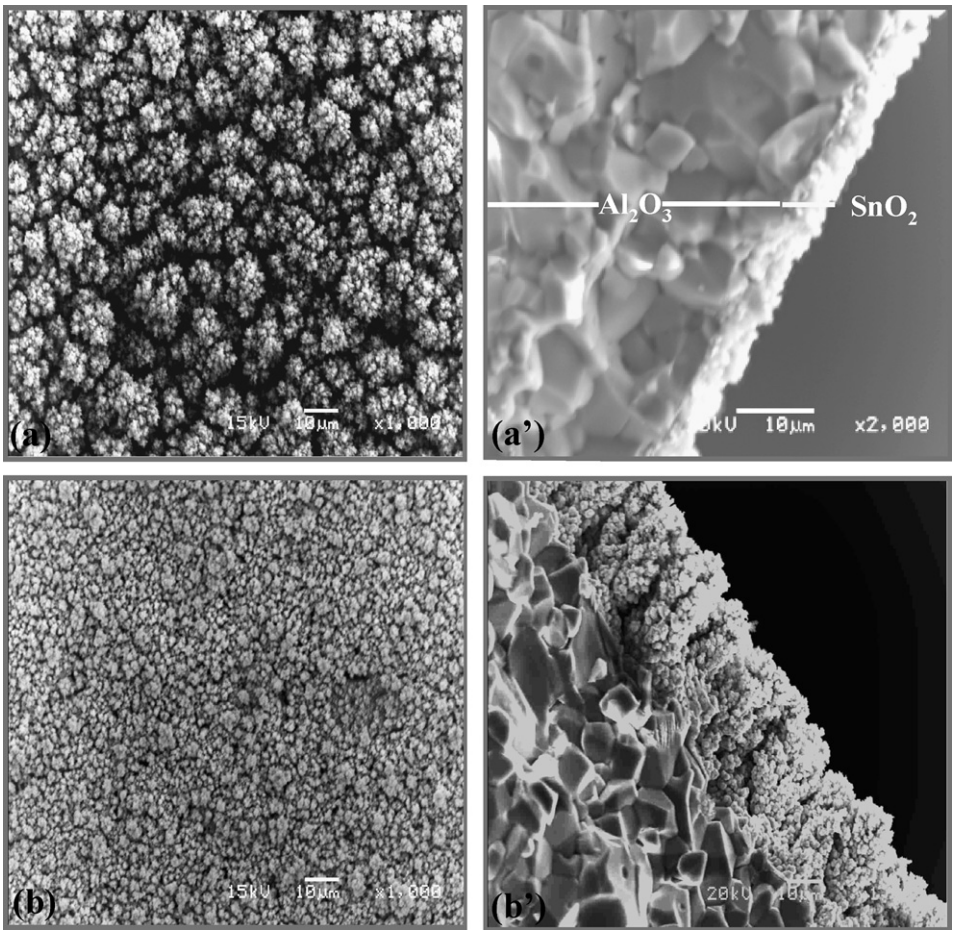

Fig. 3. SEM pictures of SnO_2 films deposited with 1 ml/h at 400 °C using different deposition times: (a) 1 h, top view; (a′) 1 h, cross-section; (b) 3 h, top view; (b′) 3 h, cross-section.

To confirm the composition of the films, EDX analysis was employed. Fig. 6 shows an EDX spectrum of SnO_2 doped with 4% of CuO realized on the marked zone from Fig. 5b. As can be seen peaks associated with Sn, Cu, and O elements are present. The other peaks noticed, i.e., C and Au peaks are due to the grid on which the sample was laid.

The XRD measurements were performed on pure and Cu-doped SnO_2 before and after annealing. The as-deposited films at 400 °C are amorphous, but annealing of these films at 550 °C in air leads to a crystalline structure. Fig. 7 displays the XRD patterns of SnO_2 and SnO_2 doped with 4% Copper. In all cases the tetragonal, rutile-type SnO_2 phase is observed and the peak positions of the films are found to be in good agreement with JCPD 77-0450. It can be noted that no shift in the SnO_2 peak positions or any Cu phase (i.e., Cu oxides or ternary compounds with Cu) is observed. This leads to the conclusion that doping of SnO_2 with Cu has occurred. There are two possible doping mechanisms of SnO_2 with Cu: substitutional and interstitial. In the case of substitutional doping some Sn^{4+} ions are replaced with Cu^{2+}(Eq. (1)) based on the comparable radii of Sn^{4+} and Cu^{2+} (0.69 and 0.73 Å, respectively). The oxygen-ion vacancies ($V_o^{\bullet\bullet}$) created by substitutional doping of Sn^{4+} with Cu^{2+} are charge compensated by electron holes ($h^{\bullet}$), if the sample is annealed in air. The electron holes compensate the Cu''_{Sn} point defects charge and are required for the site balance (Eq. (2), Kröger–Vink notations).

In the second case Cu^{2+} ions can occupy the interstitial sites of the SnO_2 lattice (Eq. (3)). As can be seen the concentration of tin ion vacancies (V''''_{Sn}) increases.

a. Substitutional:

$$CuO \xrightarrow{SnO_2} Cu''_{Sn} + O_o^x + V_o^{\bullet\bullet} \quad (1)$$

$$CuO + \tfrac{1}{2}O_2 \rightarrow Cu''_{Sn} + 2O_o^x + 2h^{\bullet} \quad (2)$$

b. Interstitial:

$$2CuO \xrightarrow{SnO_2} 2Cu''_i + 2O_o^x + 2V''''_{Sn} \quad (3)$$

The crystallite size for doped and undoped samples was calculated using the Debye–Scherrer formula[32] for the (1 1 0) peaks, i.e., $D = K\lambda/\beta\cos\theta$ where D is the crystallite size (nm), λ the radiation wavelength (0.15406 nm for Cu Kα), β the full-width at half maximum height FWHM of the X-ray line (radians) and θ is the diffraction peak angle. The average grain size D is found to be in the range 7–10 nm for SnO_2 and CuO-doped SnO_2. The XRD results confirm that the grains have a nanometer size and are in good agreement with the TEM results. In

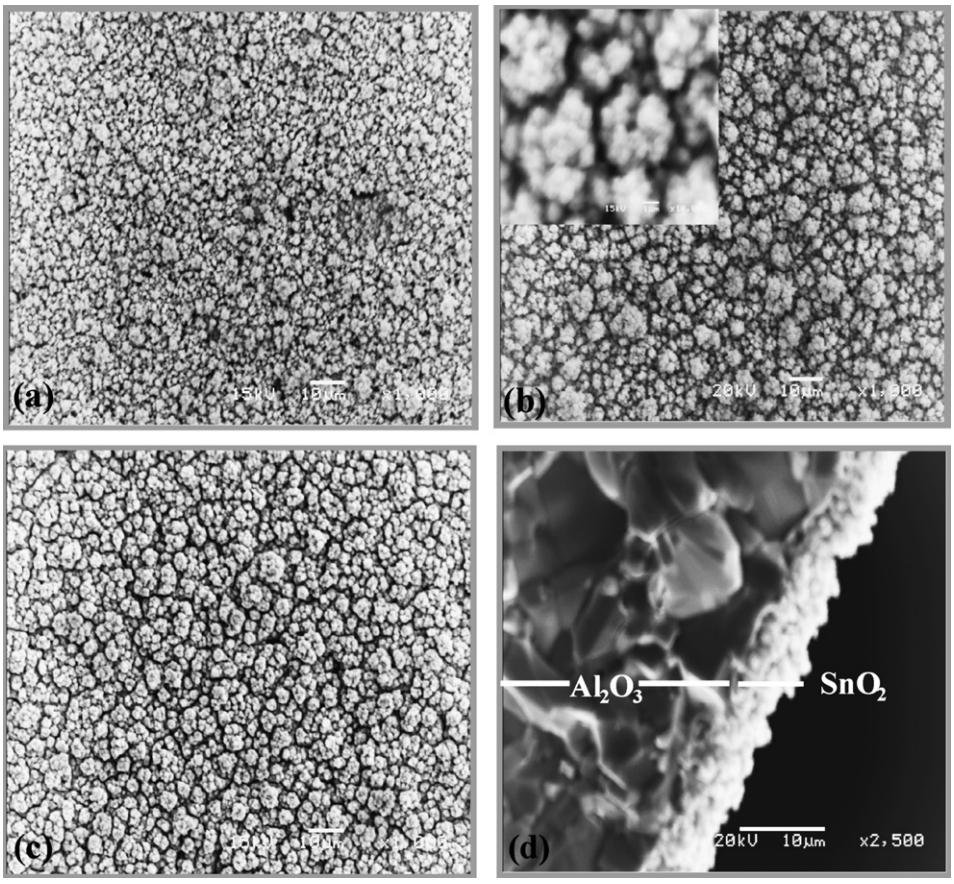

Fig. 4. SEM pictures of SnO_2 films deposited at 400 °C for 1 h using different liquid flow rates: (a) 1 ml/h; (b) 2 ml/h, top view; (c) 4 ml/h; (d) 2 ml/h, cross-section.

conclusion, the copper dopant has a minor effect on the grain size and crystallinity.

The Raman spectra of SnO_2 and Cu-doped SnO_2 films are presented in Fig. 8. The tetragonal rutile SnO_2 unit cell contains two tin ions and four oxide ions and belongs to the space group $D_{4h}^{14}(P_{42/mnm})$ and displays four Raman active modes in the bulk of SnO_2: A_{1g}, E_g, B_{1g} and B_{2g}. Three Raman peaks for SnO_2 (Fig. 8a) are detected at 474, 632, and 773 cm^{-1}, corresponding to the E_g, A_{1g} and B_{2g} vibration modes of tetragonal rutile SnO_2. These results are in good accordance with the literature values.[33] The A_{1g} (632 cm^{-1}) and B_{2g} (773 cm^{-1}) are related to the expansion and contraction vibration modes of Sn–O bonds, while E_g (474 cm^{-1}) is related to the vibration mode of oxide-ions. The B_{1g} mode corresponds to a librational motion of octahedra[34] and the intensity is very week that it is not commonly observed. Another Raman peak at 313 cm^{-1} is also observed in addition of the fundamental Raman peaks of rutile SnO_2. This Raman peak corresponds to IR active $E_u^{(3)}$TO or

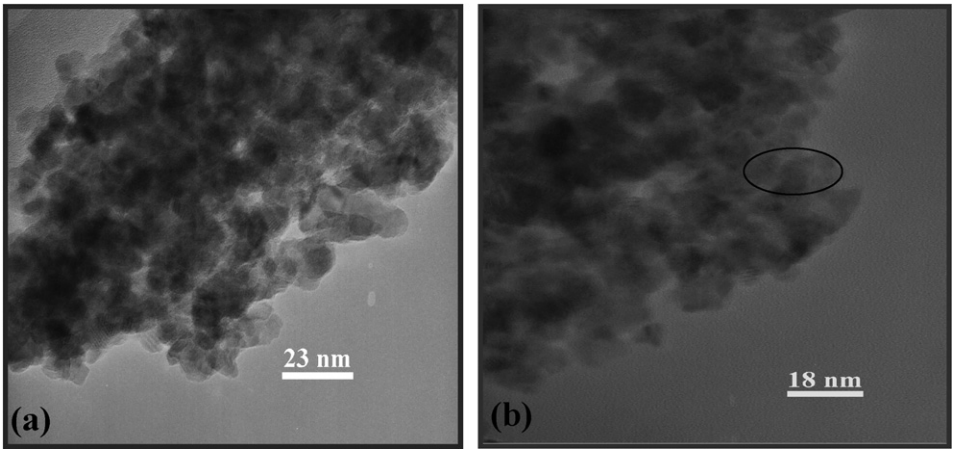

Fig. 5. TEM picture of (a) SnO_2 film and (b) SnO_2 film doped with 4% CuO deposited at 400 °C (2 ml/h for 1 h) and annealed at 550 °C for 2 h in air.

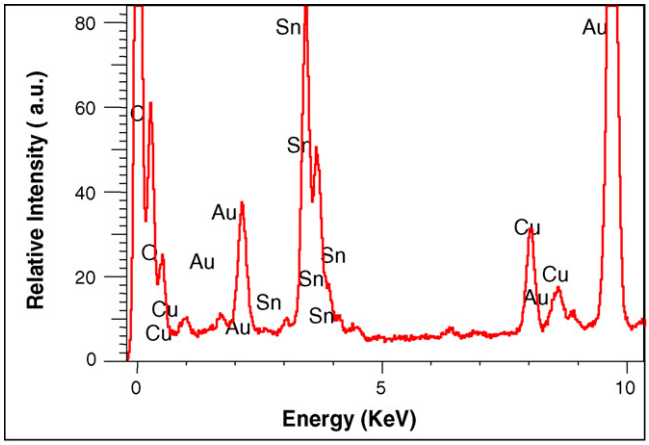

Fig. 6. EDX spectrum of SnO_2 doped with 4% CuO deposited at 400 °C (2 ml/h for 1 h) and annealed at 550 °C for 2 h in air.

$A_{2u}LO$, where TO and LO are the modes of the transverse and longitudinal optical phonons, respectively. Similar results were reported recently by Sun et al.[35] for rutile SnO_2 nanobelts and by Liu et al.[36] for rutile SnO_2 nanorods. Abello et al.[34] explained that the infrared (IR) active modes are induced when disorder and size effect takes place. Comparing the Raman spectra of the undoped SnO_2 and SnO_2 doped with different percents of CuO can be observed that for SnO_2 doped with 1% CuO (Fig. 8b) no significant shift of the peaks position takes place. In addition, an important shift of the SnO_2 A_{1g} band from 632 to 628 cm^{-1} for SnO_2 doped with 4% CuO (Fig. 8b) can be remarked. This can be ascribed to the contribution of CuO modes to SnO_2 modes taking into account that the CuO B_g mode is between 626 and 636 cm^{-1}.[37,38] Furthermore, a decrease in the intensity of the peaks with the increase of the copper percent can be remarked. Pagnier et al. attributed the decrease of the peaks to the formation of the Cu–Sn solid solution or to the stress created due to the coverage by CuO. In our case the first hypothesis can be excludes considering the XRD results but the second one can be taken into account.[39]

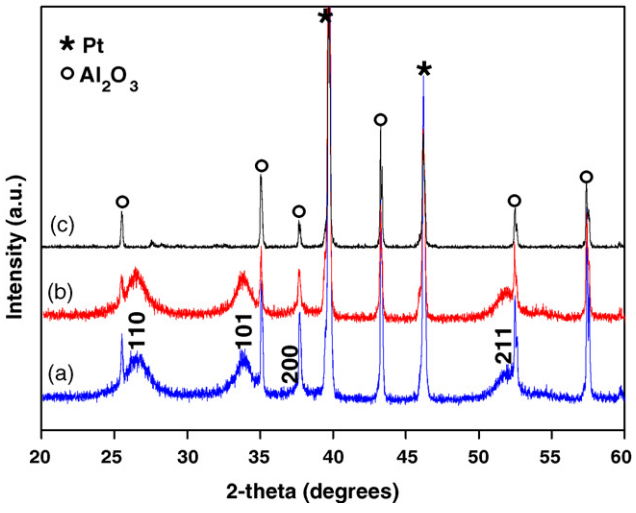

Fig. 7. XRD patterns of (a) SnO_2, (b) SnO_2 doped with 4%CuO and (c) Pt-coated alumina substrate.

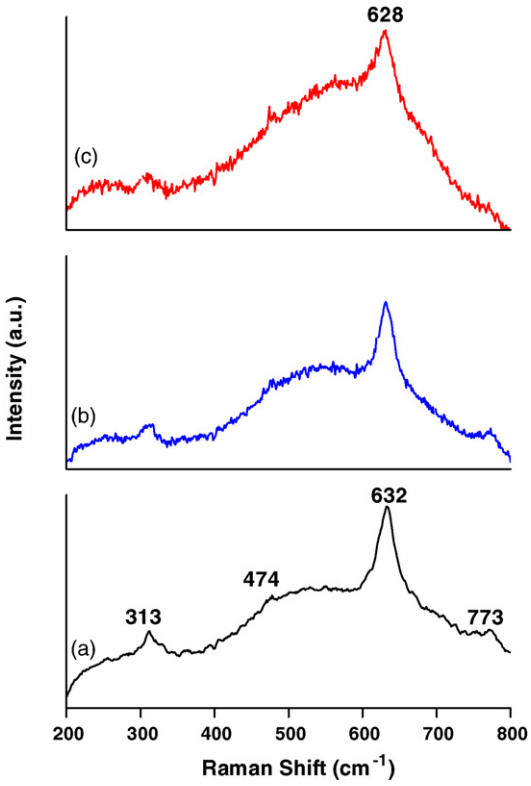

Fig. 8. Room-temperature Raman spectra of (a) SnO_2 and SnO_2 doped with (b) 1%CuO and (c) 4%CuO films deposited at 400 °C (2 ml/h for 1 h) and annealed at 550 °C for 2 h in air.

4. Conclusions

Porous nano-structured SnO_2 and copper-doped SnO_2 thin films with average particles size of 7–10 nm were successfully deposited on Pt-coated alumina substrates using electrostatic spray deposition (ESD) technique. Varying the deposition parameters (temperature, time and flow rate) SnO_2 thin films with different morphologies, thickness and particle size were obtained.

The Cu-doping proved to have minor effect on the morphology and microstructure of the SnO_2 films, as shown by SEM, TEM and XRD analysis. The Raman results confirm the rutile tetragonal phase of SnO_2. A decrease of the intensity of the bands and a shift of the A_{1g} band can be remarked when the amount of copper oxide in the film is increased.

Considering the nano-crystalline structure, the homogeneity and the porosity of these films it could be demonstrated that electrostatic spray deposition (ESD) is a useful technique to obtain thin films with desired morphology by varying the deposition parameters. Furthermore, the possibility of using these films as chemo-resistive gas sensors or in other applications can be taken into account.

References

1. Park, N.-G., Kang, M. G., Ryu, S., Kim, K. M. and Chang, S. M., Photovoltaic characteristics of dye-sensitized surface-modified nanocrystalline SnO_2 solar cells. *J. Photochem. Photobiol. A*, 2004, **161**, 105–110.

2. Yadava, Y. P., Denicoló, D., Arias, A. C., Roman, L. S. and Hümmelgen, I. A., Preparation and characterization of transparent conducting thin oxide thin film electrodes by chemical vapour deposition from reactive thermal evaporation of $SnCl_2$. *Mater. Chem. Phys.*, 1997, **48**, 263–267.
3. Chi, L.-L., Chou, J. K., Chung, W.-Y., Sun, T.-P. and Hsiung, S.-K., Study on extended gate field effect transistor with tin oxide sensing membrane. *Mater. Chem. Phys.*, 2000, **63**, 19–23.
4. Cassia-Santos, M. R., Sousa, V. C., Oliveir, M. M., Sensato, F. R., Bacelar, W. K., Gomes, J. W. *et al.*, Recent research developments in SnO_2 based varistors. *Mater. Chem. Phys.*, 2005, **90**, 1–9.
5. Leo, G., Rella, R., Siciliano, P., Capone, S., Alonso, J. C., Pankov, V. *et al.*, Sprayed SnO_2 thin films for NO_2 sensors. *Sens. Actuators B*, 1999, **58**, 370–374.
6. Rosental, A., Tarre, A., Gerst, A., Uustare, T. and Sammelselg, V., Atomic-layer chemical vapor deposition of SnO_2 for gas sensing applications. *Sens. Actuators B*, 2001, **77**, 297–300.
7. Lopes, A., Fortunato, E., Nunes, P., Vilarinho, P. and Martins, R., Correlation between the microscopic and macroscopic characteristics of SnO_2 thin films gas sensors. *Int. J. Inorg. Mater.*, 2001, **3**, 1349–1351.
8. Santos, J., Serrini, P., O'Beirn, B. and Manes, L., A thin film SnO_2 gas sensor selective to ultra-low NO_2 concentrations in air. *Sens. Actuators B*, 1997, **43**, 154–160.
9. Supothina, S., Gas sensing properties of nanocrystalline SnO_2 thin films prepared by liquid flow deposition. *Sens. Actuators B*, 2003, **93**, 526–530.
10. Matsuura, Y., Takahata, K. and Ihokura, K., Mechanism of gas sensitivity change with time of SnO_2 gas sensors. *Sens. Actuators B*, 1988, **14**, 223–232.
11. Shukla, S., Ludwig, L., Parrish, C. and Seal, S., Inverse-catalyst-effect observed for nanocrystalline-doped tin oxide sensor at lower operating temperatures. *Sens. Actuators B*, 2005, **104**, 223–231.
12. Tiburcio-Silver, A. and Sanchez-Juarez, A., SnO_2 thin films as gas sensors. *Mater. Sci. Eng. B*, 2004, **110**, 268–271.
13. Tamaki, J., Maekawa, T., Miura, N. and Yamazoe, N., CuO–SnO_2 element for highly sensitive and selective detection of H_2S. *Sens. Actuators B*, 1992, **9**, 197–203.
14. Sarry, F. and Lumbreras, M., Discrimination of carbon dioxide and fluorocarbon using semiconductor gas sensors. *Sens. Actuators B*, 2000, **67**, 258–264.
15. Delpha, C., Siadat, M. and Lumbrereas, M., An electronic nose for the discrimination of forane 134a and carbon dioxide in a humidity controlled atmosphere. *Sens. Actuators B*, 2001, **78**, 49–56.
16. Helli, O., Siadat, M. and Lumbreras, M., Qualitative and quantitative identification of H_2S/NO_2 gaseous components in different reference atmospheres using a metal oxide sensor array. *Sens. Actuators B*, 2004, **103**, 403–408.
17. Delpha, C., Lumbreras, M. and Siadat, M., Discrimination and identification of a refrigerant gas in humidity controlled atmosphere containing or not carbon dioxide: application to the electronic nose. *Sens. Actuators B*, 2004, **98**, 46–53.
18. Lee, D.-S., Kim, Y. T., Huh, J.-S. and Lee, D.-D., Fabrication and characteristics of SnO_2 gas sensor array for volatile organic compounds recognition. *Thin Solid Films*, 2002, **416**, 271–278.
19. Yang, B., Carotta, M. C., Faglia, G., Ferroni, M., Guidi, V., Martinelli, G. *et al.*, Quantification of H_2S and NO_2 using gas sensor array and an artificial neural network. *Sens. Actuators B*, 1997, **43**, 235–238.
20. Schierbaum, K. D., Weimar, U. and Göpel, W., Comparison of ceramic, thick-film and thin-film chemical sensors based upon SnO_2. *Sens. Actuators B*, 1992, **7**, 709–716.
21. Niranjan, R. S., Patil, K. R., Sainkar, R. S., Vijayamohanan, K. and Mulla, S., Morphological and sensing properties of spray-pyrolysed Th: SnO_2 thin films. *Mater. Chem. Phys.*, 2004, **84**, 37–45.
22. Korotcenkov, G., Brinzari, V., Schwank, J., DiBattista, M. and Vasiliev, A., Peculiarities of SnO_2 thin film deposition by spray pyrolysis for gas sensor application. *Sens. Actuators B*, 2001, **77**, 244–252.
23. Dima, A., Dima, O., Moldovan, C., Ciobanu, C. and Zaharescu, M., Substrate influence on the response of sol–gel derived SnO_2 gas sensor. *Thin Solid Films*, 2003, **427**, 427–431.
24. Cobianu, C., Savaniu, C., Siciliano, P., Capone, S., Utriainen, M. and Niinisto, L., SnO_2 sol–gel derived thin films for integrated gas sensors. *Sens. Actuators B*, 2001, **77**, 496–500.
25. Rella, R., Siciliano, P., Capone, S., Epifani, M., Vasanelli, L. and Licciulli, A., Air quality monitoring by means of sol–gel integrated tin oxide thin films. *Sens. Actuators B*, 1999, **58**, 283–288.
26. Lee, S. W., Tsai, P. P. and Chen, H., Comparison study of SnO_2 thin- and thick-film gas sensors. *Sens. Actuators B*, 2000, **67**, 122–127.
27. Larciprete, R., Borsella, E., De Padova, P., Perfetti, P., Faglia, G. and Sberveglieri, G., Organotin films deposited by laser-induced CVD as active layers in chemical gas sensors. *Thin Solid Films*, 1998, **323**, 291–295.
28. Sberveglieri, G., Faglia, G., Groppelli, S. and Nelli, P., Methods for the preparation of NO, NO_2 and H_2 sensors based on tin oxide thin films, grown by means of the r.f. magnetron sputtering technique. *Sens. Actuators B*, 1992, **8**, 79–88.
29. Dolbec, R., El Khakani, M. A., Serventi, A. M. and Saint-Jacques, R. G., Influence of the nanostructural characteristics on the gas sensing properties of pulsed laser deposited tin oxide thin films. *Sens. Actuators B*, 2003, **93**, 566–571.
30. Chen, C. H., Kelder, E. M., Jak, M. J. G. and Schoonman, J., Electrostatic spray deposition of thin layers of cathode materials for lithium battery. *Solid State Ionics*, 1996, **86–88**, 1301–1306.
31. Taniguchi, I., Van Landschoot, R. C. and Schoonman, J., Fabrication of $La_{1-x}Sr_xCo_{1-y}Fe_yO_3$ thin films by electrostatic spray deposition. *Solid State Ionics*, 2003, **156**, 1–13.
32. Tunstall, D. P., Patou, S., Liu, R. S. and Kao, Y. H., Size effects in the NMR of SnO_2 powders. *Mater. Res. Bull.*, 1999, **34**, 1513–1520.
33. Yu, K. N., Xiong, Y., Liu, Y. and Xiong, C., Microstructural change of nano-SnO_2 grain assemblages with the annealing temperature. *Phys. Rev. B*, 1997, **55**, 2666–2671.
34. Abello, L., Bochu, B., Gaskov, A., Koudryavtseva, S., Lucazeau, G. and Roumyantseva, M., Structural characterization of nanocrystalline SnO_2 by X-ray and Raman spectroscopy. *J. Solid State Chem.*, 1998, **135**, 78–85.
35. Sun, S. H., Meng, G. W., Zhang, G. X., Gao, T., Geng, B. Y., Zhang, L. D. *et al.*, Raman scattering study of rutile SnO_2 nanobelts synthesized by thermal evaporation of Sn powders. *Chem. Phys. Lett.*, 2003, **376**, 103–107.
36. Liu, Y., Zheng, C., Wang, W., Yin, C. and Wang, G., Synthesis and characterization of rutile SnO_2 nanorods. *Adv. Mater.*, 2001, **13**, 1883–1887.
37. Chen, D., Shen, G., Tang, K. and Qian, Y., Large-scale synthesis of CuO shuttle-like crystals via a convenient hydrothermal decomposition route. *J. Cryst. Growth*, 2003, **254**, 225–228.
38. Yu, T., Zhao, X., Shen, Z. X., Wu, Y. H. and Su, W. H., Investigation of individual CuO nanorods by polarized micro-Raman scattering. *J. Cryst. Growth*, 2004, **268**, 590–595.
39. Pagnier, T., Boulova, M., Galerie, A., Gaskov, A. and Lucazeau, G., Reactivity of SnO_2–CuO nanocrystalline materials with H_2S: a coupled electrical and Raman spectroscopic study. *Sens. Actuators B*, 2000, **71**, 134–139.